GDCh Research Article Angewandte International Edition Chemie www.angewandte.org

How to cite: *Angew. Chem. Int. Ed.* **2025**, *64*, e202414970
doi.org/10.1002/anie.202414970

Vesicles

Topological and Morphological Membrane Dynamics in Giant Lipid Vesicles Driven by Monoolein Cubosomes

Zexi Xu, Andrew Booth, Michael Rappolt, Michelle Peckham, Arwen I. I. Tyler, and Paul A. Beales**

Abstract: Lipid nanoparticles have important applications as biomedical delivery platforms and broader engineering biology applications in artificial cell technologies. These emerging technologies often require changes in the shape and topology of biological or biomimetic membranes. Here we show that topologically-active lyotropic liquid crystal nanoparticles (LCNPs) can trigger such transformations in the membranes of giant unilamellar vesicles (GUVs). Monoolein (MO) LCNPs, cubosomes with an internal nanostructure of space group *Im*3*m* incorporate into 1,2-dioleoyl-*sn*-glycero-3-phosphocholine (DOPC) GUVs creating excess membrane area with stored curvature stress. Using time-resolved fluorescence confocal and lattice light sheet microscopy, we observe and characterise various life-like dynamic events in these GUVs, including growth, division, tubulation, membrane budding and fusion. Our results shed new light on the interactions of LCNPs with bilayer lipid membranes, providing insights relevant to how these nanoparticles might interact with cellular membranes during drug delivery and highlighting their potential as minimal triggers of topological transitions in artificial cells.

Introduction

Lipid-based nanostructures are fundamental in nature, providing the structural basis of organelles that support localised intracellular and extracellular biochemical functions within living organisms.[1] These structures have inspired a range of biotechnological developments, including nanoparticulate formulations for enhanced therapeutic delivery.[2] Lipids can self-assemble into a broad array of different nanostructures dependent on their molecular shape, which gives rise to a preferred interfacial curvature in their assembled supramolecular state (Figure 1a).[3] This rich lipid polymorphism gives rise to a broad range of tuneability in the properties of lipid-based formulations.[2a,3a] Curved 3-dimensional (3D) lipid nanostructures known as cubosomes have been of particular recent interest; their high interfacial surface area gives a high capacity for drug loading and interfacial chemical processes within an individual nanoparticle.[4] It has also been reported that inverted cubic phases can promote membrane fusion and topological transitions by contributing to the spontaneous formation of transient pores, closely resembling structural intermediates observed in the topological transformations of cellular membranes.[5] Therefore cubosomes are of broad interest within nanomedicine and bottom-up approaches to synthetic biology through the design of artificial cells. The internal structure of cubosomes consists of highly curved lipid bilayers draped around a periodic minimal surface creating two distinct continuous 3D-networks of water channels (Figure 1b).

Real cells and many artificial cells are bound by a lipid bilayer membrane as their intrinsic structural matrix. Therefore understanding the interactions between lipid cubic phases and lamellar lipid bilayer structures is fundamental to improving our understanding of drug delivery mechanisms and potential bioengineering applications within artificial cells. Essential to the functionality of biological membranes is their ability to undergo dynamic shape and topology transformations involved in critical cell activities such as growth, division and trafficking.[6] In nature, a range of protein complexes are involved in the regulation of these membrane remodelling events by a range of active and passive interaction mechanisms that scaffold, bend and cut the membrane as required, including the BAR (Bin-Amphiphysin-Rvs) proteins, ESCRTs (endosomal sorting complex required for transport), SNAREs (soluble N-ethylmaleimide-sensitive fusion protein attachment protein receptors), caveolin, dynamin and cytoskeletal filaments.[7] The fluidity and flexibility of these interfacial membrane structures are key to these processes. The energy barriers to topological transitions are regulated by lipid composition and the intrinsic curvature stress stored within these

[*] Z. Xu, M. Rappolt, A. I. I. Tyler
School of Food Science and Nutrition, University of Leeds, Leeds, LS2 9JT, United Kingdom
E-mail: A.I.I.Tyler@leeds.ac.uk

Z. Xu, A. Booth, P. A. Beales
School of Chemistry and Astbury Centre for Structural Molecular Biology, University of Leeds, Leeds, LS2 9JT, United Kingdom
E-mail: P.A.Beales@leeds.ac.uk

M. Peckham
School of Molecular and Cellular Biology and Astbury Centre for Structural Molecular Biology, University of Leeds, Leeds, LS2 9JT, United Kingdom

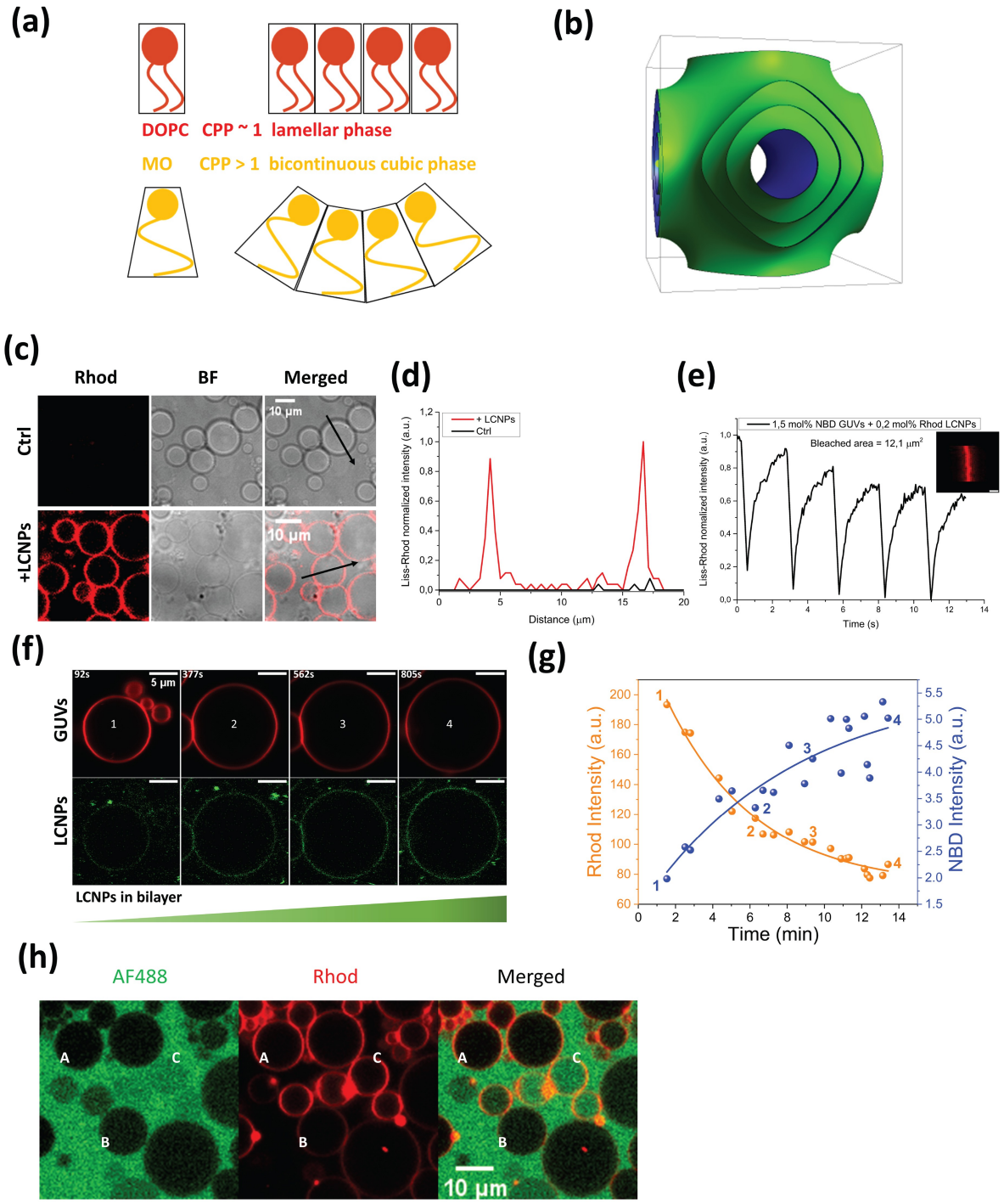

Figure 1. (a) Schematic depicting the molecular shapes of DOPC and MO, their critical packing parameters (CPP) and preferred self-assembled structures; (b) The minimal surface of the primitive *Im3m*bicontinuous cubic phase; (c) The incorporation and homogeneous distribution of Rhod-PE labelled LCNPs (red) on the surface of NBD-PE labelled GUVs. BF = bright field; (d) Line intensity profiles before and after addition of Rhod-PE labelled LCNPs. The normalized Rhod-PE fluorescence is based on the maximum intensity of Rhod-PE in the LCNPs-GUVs sample; (e) FRAP recovery curves of Rhod-PE diffusion in DOPC GUVs following the addition of Rhod-PE labelled LCNPs. (f) Real-time observation of NBD-PE labelled LCNPs incorporation into Rhod-PE labelled GUV membranes; (g) NBD-PE intensity increases while Rhod-PE intensity decreases with time; (h) GUVs labelled with Rhod-PE with different degrees of permeability to 10 kDa dextran labelled with AF488: unleaked (< 20% fluorescence leakage) GUV (A), partially leaked (20 to 80% fluorescence leakage) GUV (B), and fully leaked (> 80% fluorescence leakage) GUV (C).

membranes, where the shape of lipid molecules influence the lateral stress profile across a bilayer membrane.[8] There-

fore seeding lipid bilayer membranes with curved lipid structures such as cubosomes has the potential to enhance their topological activity.

The interaction of lyotropic liquid crystal nanoparticles (LCNPs) such as cubosomes with different surfaces and cells has been extensively studied.[9] Of particular interest are their interactions with lipid membrane interfaces, where insight has previously been provided using solid-supported lipid bilayers.[10] These studies suggest a strong and rapid attraction between LCNPs and supported DOPC lipid bilayers on silica.[10b] Once sufficient LCNPs incorporate into the supported bilayer, this leads to destabilisation of its structure and a net release of material from the bilayer; quartz crystal microbalance with dissipation (QCM–D) monitoring revealed the lipid surface becomes viscoelastic with a large change in dissipation following addition of LCNPs.[10b] Moreover, a significant lipid exchange between hydrogenated monoolein (MO) LCNPs and a deuterated DOPC lipid bilayer was confirmed by neutron reflectivity, revealing bidirectional transfer of MO to the supported bilayer and DOPC to the LCNPs.[10b] By contrast, the incorporation of LCNPs into supported bilayers was hindered in more organised lipid bilayers in the gel phase, where dipalmitoylphosphatidylcholine (DPPC) lipids densely pack in an orthorhombic fashion.[11] Complementary small angle X-ray scattering (SAXS) results confirmed that LCNPs have a strong interaction with DOPC unilamellar and multilamellar vesicles: large changes in the unit cell dimensions of the LCNPs were observed, eventually resulting in a transition from a cubic to lamellar phase structure once DOPC and MO mix.[11]

Insights into the interactions of LCNPs with bilayer membranes have also been gained from cell interaction studies.[9b,12] MO-LCNPs stabilised by either Pluronic F127 or F108 copolymers were observed to alter the lipid distribution and membrane structures of HeLa cells, resulting in lipid droplet accumulation, mitochondrial hyperpolarization and mitochondrial reactive oxygen species (ROS) generation.[13] Furthermore, Dyett et al. observed individual MO-LCNPs interact with the cell membranes of small intestine epithelial cells and STO fibroblast stem cells by docking onto the membrane surface before diffusing into the membrane, suggestive that the MO incorporates into the cell membrane structure,[9c] analogous to reported interactions with minimal model membrane systems.[10a,11]

Current studies have shown strong evidence for the interaction and mixing of LCNPs with bilayer membranes with synergies between findings in model membranes and live cells. However, studies in cell-sized unsupported model membranes are missing that would provide greater fundamental insight into the dynamic processes that might occur in unsupported membranes seeded with topologically-active MO-LCNPs. Here we bridge this gap by applying time-resolved confocal fluorescence and lattice light sheet microscopy to study the interaction between MO-LCNPs and DOPC-GUVs and the dynamic processes during re-equilibration. We reveal a rich diversity and interplay of membrane topological and shape changes that mimic many of the processes of living cellular membranes. These findings shed new light on the potential cellular interaction mechanisms of LCNPs in drug delivery systems as well as underpin the potential of LCNPs as topologically active triggers for membrane remodelling events in artificial cell technologies.

Results

Incorporation of MO from LCNPs into the lipid bilayer causes GUV growth

LCNPs composed of MO stabilized by Pluronic F127 were assembled by hydration of a dried lipid film and sonication. SAXS measurements demonstrated that the LCNPs were in the *Im*3*m*inverse bicontinuous cubic phase (Figure S1a). Figure 1b shows the 'primitive' minimal surface with the crystallographic space group *Im*3*m*. LCNPs had an average hydrodynamic diameter of 179 ± 19 nm and a polydispersity index (PDI) of 0.172 ± 0.005, determined by dynamic light scattering (DLS) (Figure S1b). Cryogenic transmission electron microscopy (cryo-TEM) revealed the structure of the dispersed LCNPs, with a fast Fourier transform (FFT) image analysis, confirming the internal *Im*3*m*crystal structure (Figure S1c).

An initial LCNP concentration screen between 0.95 and 6.7 mg/ml MO mixed with DOPC GUVs using confocal fluorescence microscopy revealed a range of behaviours from rich morphological transformation in the GUVs at low concentration, seen after approximately 2 to 5 minutes, to significant destabilisation and destruction of GUVs at high concentration. From this initial screen, a LCNP concentration of 1.4 mg/ml MO and a MO/DOPC molar ratio of ~250 was selected for further investigation as, under these conditions, rich structural changes were observed in the GUVs over the experimental time window of approximately 20–30 min. We note that the general vesicular architectures of GUVs were stable within the studied time frame.

LCNPs were found to incorporate within the membranes of GUVs. LCNPs first labelled with 1,2-dioleoyl-*sn*-glycero-3-phosphoethanolamine-N-(lissamine rhodamine B sulfonyl) (ammonium salt) (Rhod-PE) were mixed with 1,2-dioleoyl-*sn*-glycero-3-phosphoethanolamine-N-(7-nitro-2–1,3-benzoxadiazol-4-yl) (ammonium salt) (NBD-PE) labelled DOPC GUVs (1.4 mg/ml MO and MO/DOPC $\approx$ 250 mol/mol). A uniform signal from the LCNPs was observed at the GUVs membrane surface, indicating that the lipid components of the LCNPs had incorporated within the bilayer structure of the GUVs, as simple adsorption of LCNPs on the GUV surface would be observed as punctate spots of fluorescence at the GUV membrane (Figure 1c). Fluorescence intensity line profiles of Rhod-PE across GUVs show a uniform fluorescence signal from the membrane after interaction with LCNPs compared to the control samples (Figure 1d). Fluorescent recovery after photobleaching (FRAP) experiments show rapid and reproducible recovery of Rhod-PE fluorescence over ~5–15 μm^2 areas of membrane consistent with the fluidity of lipid bilayer membranes (lateral diffusion constant, $D \approx \mathcal{O}(\mu m^2 s^{-1})$) (Figure 1e; Figure S2). This is in agreement with previous studies, showing that LCNPs can

adsorb into the DOPC membrane surface.[10,14] Figure S3 also shows the incorporation of NBD-PE labelled LCNPs on Rhod-PE labelled GUVs, and Rhod-PE labelled LCNPs on unlabelled GUVs to confirm the LCNPs-GUVs interaction. The incorporation kinetics was investigated using LCNPs labelled with NBD-PE and GUV membranes labelled with Rhod-PE. Figure 1f, g show that over 13 min, the Rhod-PE probe intensity in the GUV membranes decreased, as it was diluted by MO lipids that fused into the membrane structure (Figure 1g). A proportional increase in NBD-PE fluorescence intensity at the GUV membrane correlates with this Rhod-PE intensity decrease. The GUV membrane surface area is also seen to increase in a correlated GUV growth process. For example, in Figure 1f, the apparent GUV diameter increased by a factor of 1.4 in 14 min, which corresponds to the surface area increasing by a factor of ~2. Consistent with this observed GUV growth, the dilution of Rhod-PE in the membrane showed a decrease in fluorescence intensity by a factor of ~2.2. The LCNP-GUV fusion mechanism must therefore distribute MO relatively evenly to both monolayers of the GUV membrane, otherwise significant morphological effects would be expected to be observed long before this swelling ratio is reached due to significant stresses that would be generated by transmembrane asymmetry.

Although no clear correlation was found between GUV swelling and leakage, occasional leakage of GUVs was observed following the addition of LCNPs, suggesting a potential increase in membrane permeability (Table S1). A membrane-impermeable dextran (10 kDa) labelled with Alexa Fluor 488 (AF488) or Cascade Blue (CBlue) was added to the extra-vesicular medium. These passive membrane permeability probes were observed to leak into the lumen of the GUVs over time. GUV leakage to these probes was observed to be stochastic and hence variable between different GUVs in a sample, evident by the different degrees of dextran leakage shown in Figure 1h with unleaked, partially leaked and fully leaked GUVs. Further evidence for the stochastic enhanced permeability of the GUVs induced by MO lipids can be seen in the correlation between vesicle growth (or swelling) and the onset of vesicle leakage (Figure S4).

Generally, GUV permeabilisation occurs near-simultaneously or with a lag time compared to GUV growth from the fusion of MO lipids into the bilayer structure. We attribute the influx of large macromolecules such as 10 kDa dextran into the lumen of the GUVs to be induced by the stochastic formation of pores in the vesicle membrane.[15] This is likely due to the enhanced curvature elastic stress in the GUV membranes due to the non-bilayer preferring MO lipids, which favour highly curved structures such as toroidal pores. The resistance to leakage by some GUVs in the sample is suggestive that an energy barrier needs to be overcome for pore formation and that the probability of pore formation is dependent on GUV membrane composition (variability in DOPC:MO ratios across the GUV population).[9a,c] After the GUVs were observed to swell during a growth process induced by MO incorporation, a stability limit appeared to be reached, beyond which a rich array of morphological transitions was observed in the GUVs.

MO LCNPs bring DOPC GUVs to life by triggering a cascade of dynamic shape and topological transformations.

Incorporation of MO-LCNPs into DOPC-GUVs is expected to create a significant stored curvature elastic stress in the membranes. Non-bilayer-forming MO lipids (spontaneous curvature $= -0.054 \pm 0.003$ Å^{-1}) have an inverted cone shape that prefers curved membranous interfaces,[16] such as in the *Im3m*cubic phase. This contrasts with the near-cylindrical shape of DOPC lipids (spontaneous curvature $= -0.0091 \pm 0.0008$ Å^{-1}) that preferentially aggregate as planar bilayer membranes.[17] Increasing concentration of MO lipids in the GUV membrane enhances the lateral pressure profile in the hydrophobic core of the bilayer such that each lipid monolayer wants to bend towards the hydrating aqueous medium. Once the MO concentration reaches a critical threshold, these stored stresses are observed to release through a range of GUV morphological transitions.

Nanotubes

Within a few minutes following the addition of LCNPs to DOPC GUVs, the majority of vesicles developed a topologically-invariant shape transformation that manifests as lipid tubes protruding from the membrane. These tubes varied in size and direction (into the extra-vesicular medium or the interior lumen). Thin cylinder-like (Figure 2a) and thick unduloid-like (Figure 2b) external nanotubes were observed to protrude from the parent GUV toward the extra-vesicular medium. We also observed internal lipid nanotubes originating at the surfaces of the GUV and protruding into the vesicle lumen (Figure 2c). Both external and internal tubes are undulating and wavy, while some of them form an undulatory pearling pattern. Dynamic fluctuations in all morphologies of both external and internal tubes were observed, suggesting that the incorporation of MO into the DOPC membrane facilitates the membrane to be highly flexible. In addition, the fluorescence of water-soluble membrane permeability probes in the internal nanotubes indicates that they have an open neck that connects to the extra-vesicular medium (Figure 2c).

Previous studies have reported the pearling instability of GUV nanotubes when the membrane is subject to tension caused by bilayer asymmetry.[18] In our experiments, it is unclear whether LCNP fusion into the GUVs creates bilayer asymmetry or not. Asymmetry exists in terms of the LCNP interaction with the GUV membrane, which is exclusively from the extra-vesicular side of the membrane. However, the rate of MO flip-flop across the bilayer is unknown and any potential asymmetry cannot be resolved from our fluorescence microscopy methods. Lipid flip-flop may occur through collective formation of transmembrane pores, which we sometimes observe after a lag time following GUV growth. Pearling instabilities were mostly observed in

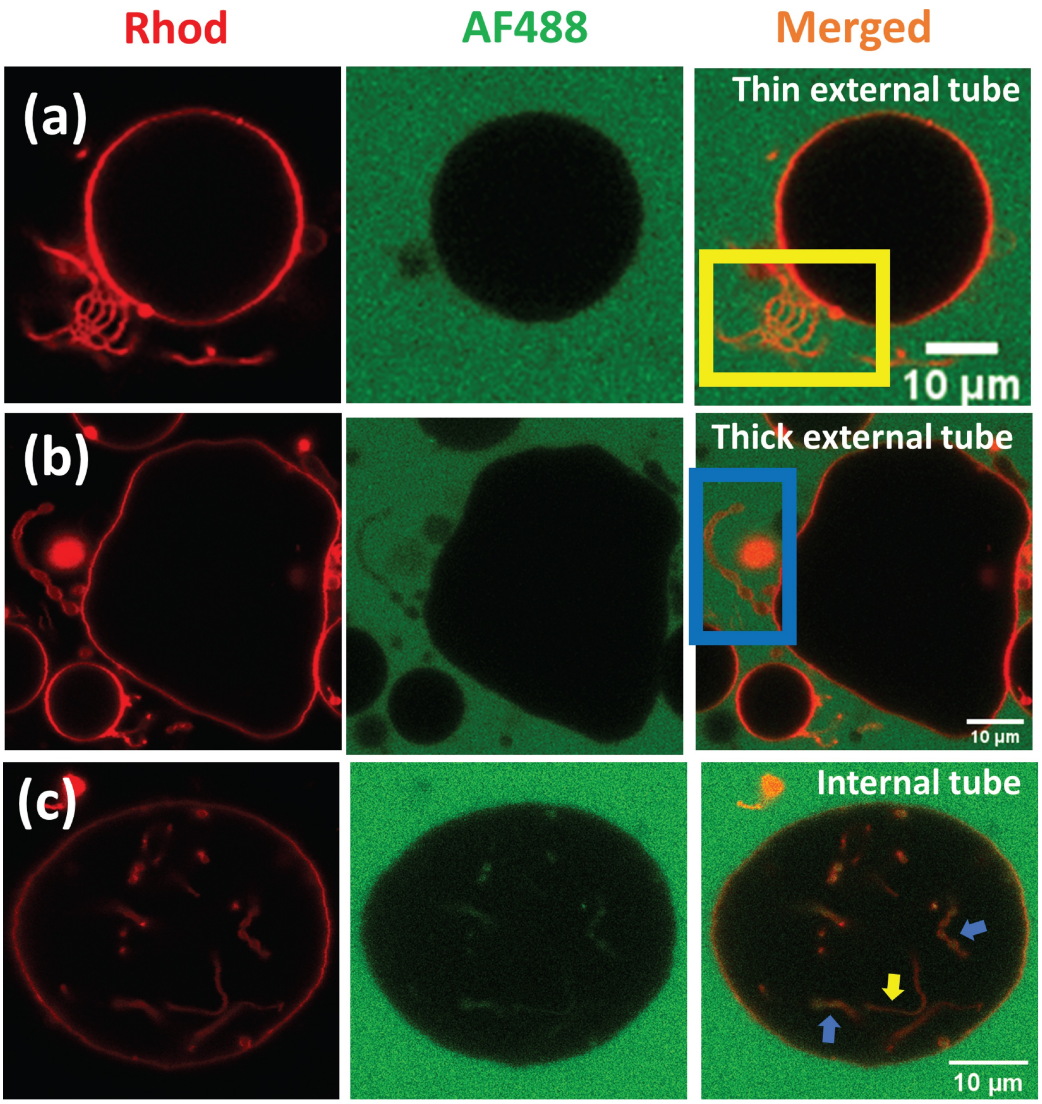

Figure 2. Membrane tubulation following initial growth of GUVs after being fed with MO LCNPs. Thin (a) and thick (b) external lipid nanotubes protrude from vesicles toward the extravesicular medium; (c) thin (yellow arrows) and thick (blue arrows) internal lipid nanotubes that have originated at the surfaces of the GUVs and protrude into the vesicle lumen. Membrane-impermeable dextran (10 kDa) labelled with AF488 (green) was observed in the internal nanotubes.

unleaked GUVs. Therefore, we speculate that asymmetric membrane stresses from enhanced MO localisation in the outer membrane monolayer of GUVs drives the pearling of lipid tubules that are observed.

Fusion and fission

GUV fission and fusion events were also observed following the addition of LCNPs. To study these topological transformations in more detail, two populations of DOPC GUVs labelled with different fluorescent probes were mixed prior to the addition of LCNPs. The two distinctly labelled populations of GUVs can therefore report on lipid mixing phenomena between adjacent vesicles. One GUV population was labelled with 3,3′-Dioctadecyloxacarbocyanine Perchlorate (DiO; green) and the other GUV population was labelled with Rhod-PE (red, as above).

A typical GUV fusion event is shown in Figure 3a. The contact area between two neighbouring GUVs increases without any observable lipid mixing between the two GUVs. A full fusion pore then opens and the interior lumens of the GUVs mix. This is followed by reconfiguration of the combined GUVs into a single spherical vesicle, where the red and green lipid probes become evenly mixed throughout the membrane by lateral diffusion. Lipid nanotubes that can be seen in the two initial vesicles are conserved within the lumen of the initial fused GUV. However, these tubes disappeared within 2 min of the fusion event, likely retracting into the GUV membrane as the lipid mixture re-equilibrates.

Other fusion-related mechanisms were observed. An example is shown in Figure 3b (Movie S1), where a GUV

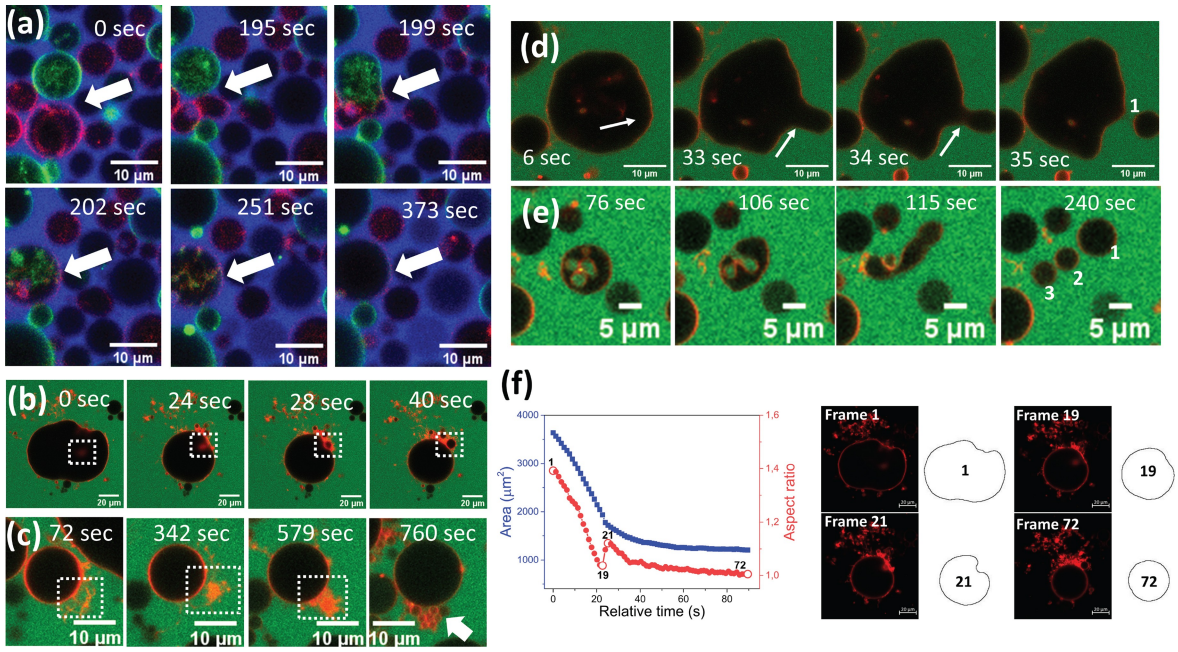

Figure 3. LCNPs trigger fusion and fission events between GUVs or lipid nanotubes: (a) Full fusion of two individual vesicles labelled with DiO (green) and Rhod-PE (red) respectively; (b) An internal vesicle fuses with the outer GUV before translocating to the vesicle exterior; (c) The formation of several small spherical vesicles from the fusion of external lipid nanotubes; (d) The "mother" vesicle generates one smaller GUV; (e) The "mother" vesicle separates into three smaller GUVs; (f) Kinetics of GUV re-equilibration to a spherical shape. Graph of GUV surface area and aspect ratio vs time (left). Representative GUV images from Movie S1 and the extracted GUV outline (right).

"gives birth" to a smaller GUV from its interior lumen. The interior GUV adheres to the membrane of the outer GUV before translocating to the exterior of this vesicle within a few seconds. We speculate that the internal GUV becomes hemifused with the outer membrane to facilitate this translocation event. It should also be noted that the outer GUV is initially non-spherical and gradually loses its large excess membrane area to become near-spherical during the time course of our observation window (~2 min).

Fusion can also occur between external lipid nanotubes that initially formed on the GUV surface. These tubes have been observed to fuse with one another on a time scale in the order of 10 min, resulting in the formation of many smaller, spherical GUVs (Figure 3c).

Analogous to membrane fusion, membrane fission was also observed. The excess membrane area induced by fusion of LCNPs into the GUV membrane can lead to membrane buds that fission and divide into daughter GUVs (Figure 3d, Movie S2). The large excess area and dynamic shape transformations in these vesicles can also lead to vesicles fissioning into multiple daughter GUVs as they re-equilibrate to a spherical GUV geometry (Figure 3e).

Following fusion of LCNPs into GUV membranes, relaxation of fluctuating GUVs with a larger excess membrane area to re-equilibrate back to a near-spherical GUV structure is commonly observed. We characterise the time course of one such GUV in Figure 3f (Movie S1) in terms of the apparent membrane area and vesicle aspect ratio ($AR = \frac{major\ axis}{minor\ axis}$) over time. The GUV gradually reduces its membrane area and aspect ratio on the time scale of order 80 s until the aspect ratio returns to approximately 1.0 (spherical shape).

Intraluminal vesicles (ILVs)

Membrane topological changes through fusion and fission processes can lead to the generation of new internal lipid compartments inside GUVs: intraluminal vesicles (ILVs). To investigate ILV formation, where extra-vesicular media is encapsulated within these new compartments, a membrane-impermeable 10 kDa dextran labelled with AF488 or CBlue was added to the bulk medium. Formation of ILVs is characterised by the inclusion of AF488 or CBlue in the lumen of these internal vesicles.

We observed three different pathways for ILV formation, summarised in Figure 4. In Figure 4a (Movie S3), internal lipid nanotubes that include the external CBlue probe remodel into discrete ILVs that also encapsulate CBlue from the bulk medium. A second mechanism saw two separate GUVs undergo a fusion mechanism, where two independent fusion pores form in the adhesion contact area, such that the membrane in the adhesion plaque becomes scissioned inside the new GUV and encapsulates the AF488 probe (Figure 4b, Movie S4). A final ILV formation mechanism was observed when a non-spherical GUV with larger excess membrane area undergoes membrane fluctuations that lead to a discocyte GUV shape folding around such that the spheroidal end-caps of this structure contact and fuse. This topological transition leaves a CBlue-

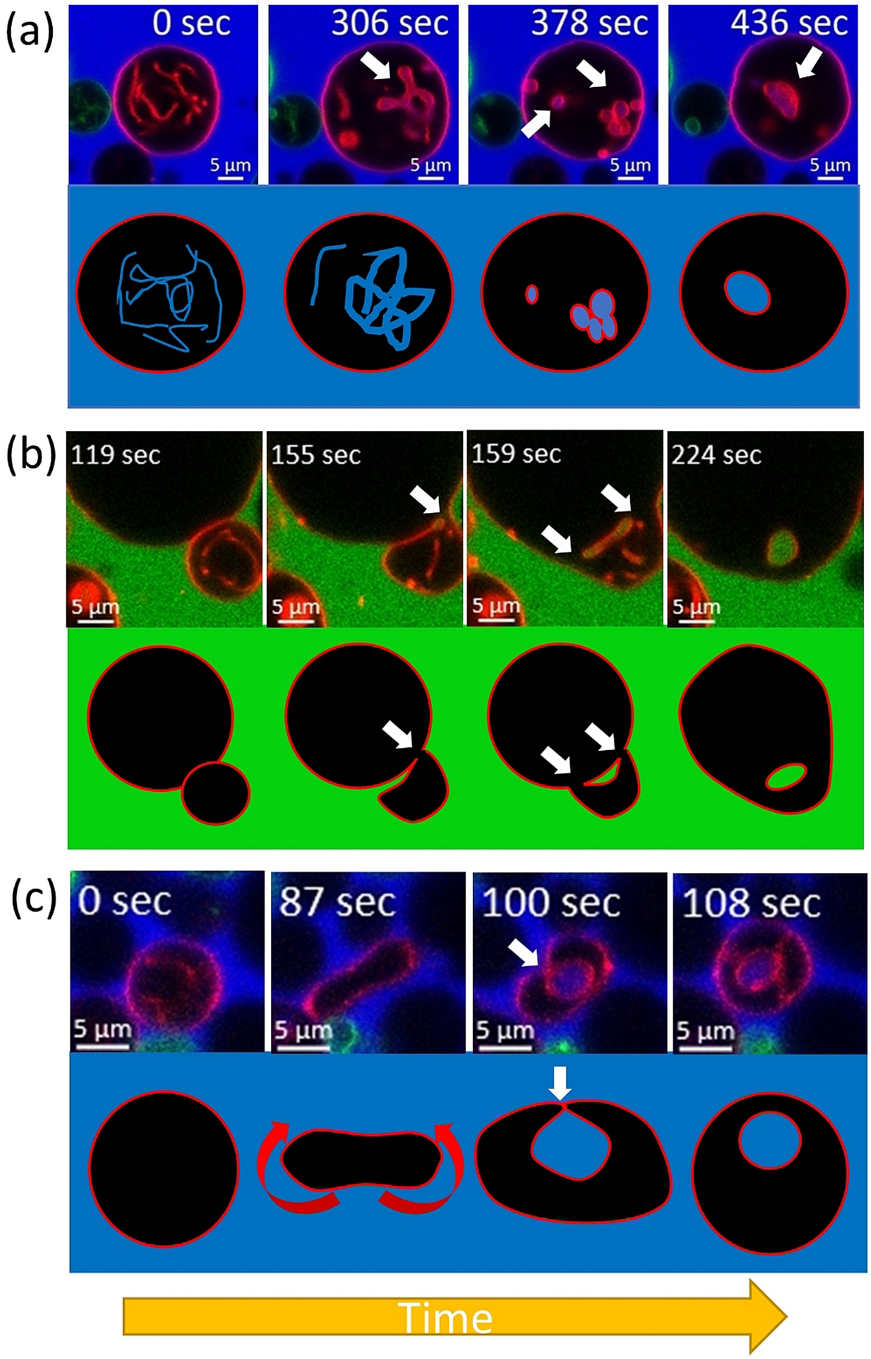

Figure 4. Intraluminal vesicles can form by different mechanisms. (a) Internal nanotubes fuse to form ILVs. White arrows indicate thin tubes that first fuse to form thicker tubes before forming small ILVs, which continue to fuse into a larger ILV. (b) Two individual vesicles fuse in a mechanism that leads to a trapped ILV. White arrows indicate fusion at each edge of the membrane contact area during fusion. (c) Wrapping of a discocyte GUV leads to fusion of the end caps and formation of an ILV. Red arrows represent the movement of the vesicle and white arrows show fusion of the membrane. In all cases, ILVs are filled with external medium that contains the membrane-impermeable AF488 or CBlue dextran (10 kDa).

encapsulating ILV trapped inside an outer membrane (Figure 4c, Movie S5). Lattice light sheet data further demonstrated these fusion and fission events in 3D, confirming the topological and morphological transformation of GUVs (Figure 5a, Movie S6, S7).

Buds

The final re-equilibrated state of the GUVs often resulted in remaining excess membrane area being taken up in membrane buds at the GUV surface. These small buds often have a high fluorescence intensity, suggesting that they may be multilamellar structures (Figure 5b). The estimated

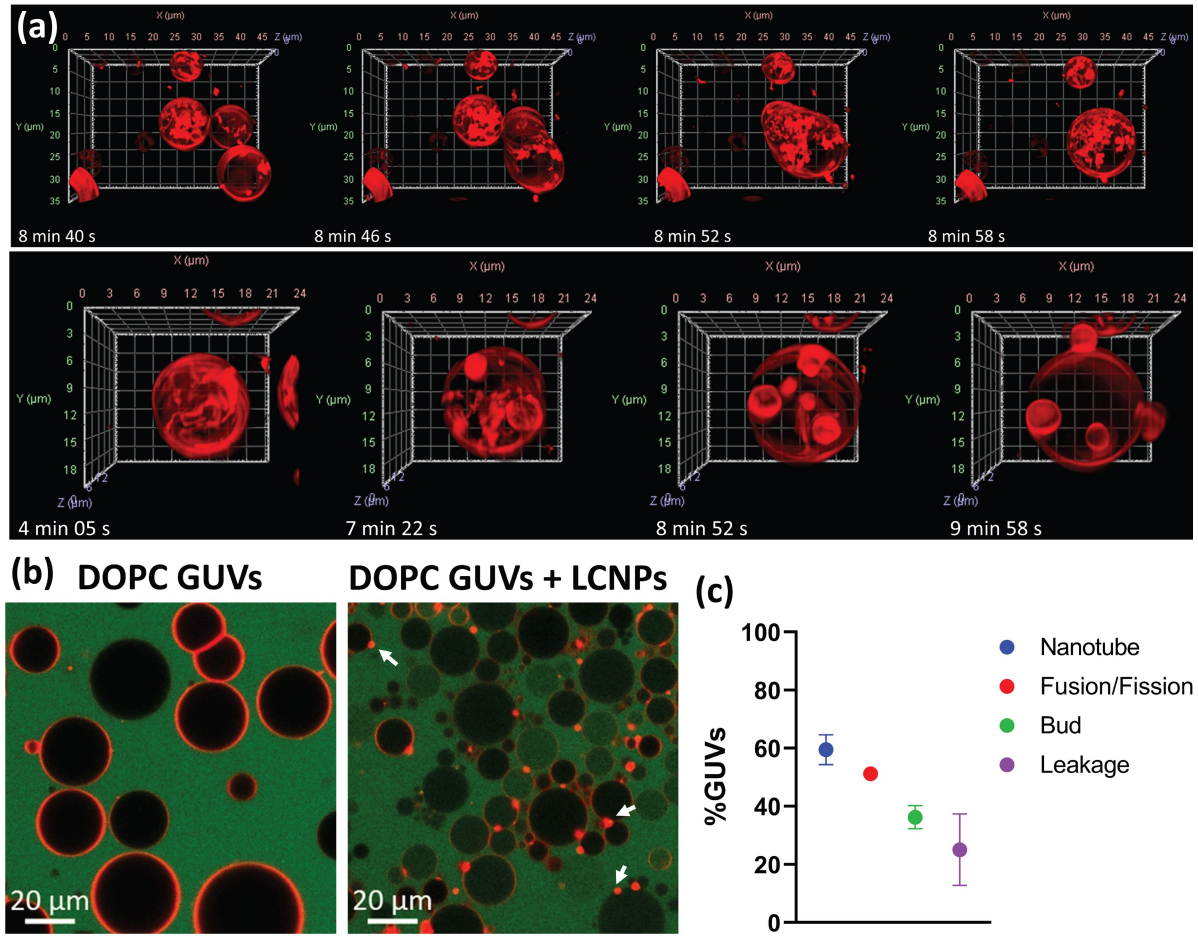

Figure 5. Lattice light sheet images of (a) Fusion of three GUVs (top, movie S6) and intraluminal vesicles formation by the fusion of internal nanotubes (bottom, movie S7). The greater depth of 3D imaging accessible by lattice light sheet microscopy provides further evidence of the topological transformations of GUVs induced by LCNPs. (b) DOPC GUVs before (left) and after (right) LCNPs addition. Following equilibration after LCNP addition, red buds with high fluorescence intensity were observed at the edge of GUVs (white arrows indicate some example buds within the image). (c) Statistical analysis percentage of nanotubes (blue) and fission/fusion (red) (n = 362); buds (green) and leaked GUVs (purple) (n = 374) within ~20 min. Data are presented as the mean ± S.D.

composition of the MO and DOPC mixture in these buds would favour lamellar structures, based on previous SAXS and neutron reflectivity experiments[10a,11] (note, the MO to DOPC ratio was about 43 mol %; see also discussion below). Neutron scattering studies have revealed an initial rapid adsorption of intact LCNPs at the DOPC bilayer interface, followed by exchange of lipids. Furthermore, SAXS measurements confirmed the strong interaction between LCNPs and DOPC vesicles including unilamellar and multilamellar that initially leads to changes in the size of the unit cell of the cubic phase before transition to a lamellar structure (DOPC/MO molar ratio of 0.01–0.18).[11]

Prevalence of the different observed shape and topology transitions

The LCNPs triggered a variety of shape and topological transformations in the GUVs including fusion/fission, pore formation, tubulation and membrane budding. Control experiments show that neither PBS (phosphate-buffered saline) buffer, F127 stabilizer, nor DOPC nanoparticles induce these morphological changes on GUVs (Figure S5). Therefore MO is critical in inducing the observed effects. A further control experiment involved the addition of 1:1 DOPC:MO multilamellar vesicles (MLVs) (Figure S6). Here, no effect on the GUVs was observed after 10 min. After 30 min, some morphological effects on GUVs were observed, such as tubulation and GUV aggregation, but no evidence of topological changes in the GUVs was observed. This is suggestive that the cubosome structure is important to increase the kinetics of fusion with GUVs, enhancing the rate of MO transfer and leading to morphological changes in GUVs on shorter time scales. Furthermore, while some morphological effects were eventually observed after longer incubation times, these were milder effects than observed for MO LCNPs. This indicates that the ratio of MO:DOPC in the GUVs is important to access some of the more notable topological effects, which is most readily achieved with the pure MO LCNPs with an inner *Im3m* cubic structure.

A statistical analysis of MO LCNP-induced events was performed, analysing 362 GUVs for fusion/fission (including ILV formation) and nanotube formation events. 357 GUVs were analysed for membrane permeability and budding events. These data are reported as the mean ± standard deviation (S.D.) from at least three independent experiments at a time point 20 min after addition of LCNPs. In summary, 60±5 % GUVs contained nanotubes and 51.2± 1.3 % GUVs had fusion/fission events, 36±4 % GUVs contained buds and 25±12 % GUVs formed membrane pores that rendered the membranes permeable to the fluorescent probe in the extravesicular medium (Figure 5c). It should be noted that, except for leakage, these percentages are an underestimate, as additional events will be happening above and below the plane of confocal imaging that were unobserved.

Discussion

Topological changes in an object occur under extreme conditions, which require the 'ripping' or 'gluing' of the object that cannot be achieved under smooth shape transformations. Topological transformations of lipid vesicles include fission, fusion and pore formation events, where the topology is defined by its Euler characteristic (χ).[19] The Euler characteristic can be defined in terms of the Betti numbers (b_n), where b_0 is the number of objects, b_1 is the number of circular holes, b_2 is the number of internal voids and $\chi = \sum_{i=0}^{n} (-1)^i b_i$, where $b_i = 0$ for $i \geq 3$.[20] Common topological transformations of lipid vesicles along with their Euler characteristic and Betti numbers are shown in Figure 6a. Note that a vesicle with a pore has the same topology as a 2D planar bilayer sheet. The Gaussian curvature contribution to the energy change between topological states is given by $E_G = 2\pi\kappa_G\Delta\chi$, where the Gaussian modulus, κ_G, is negative, and hence, this contributes to an energetic benefit for transitions to topological states with increasing Euler characteristic, if the change in bending energy between these states is small.[19] However, significant energy barriers exist to the molecular rearrangements between these structures, which usually prevent them from occurring spontaneously. These energy barriers can be reduced by the inclusion of lipids that prefer curved interfaces, which impart curvature stresses and modulate the elastic energies of the membrane. Therefore MO lipids, which preferentially form an *Im3m*cubic phase with $\chi = -4$,[21] have strong potential to seed bilayer membranes with the propensity to undergo topological and shape changes.

We have observed a rich variety of morphological and topological transitions in DOPC GUVs induced by MO-LCNPs in the *Im3m* cubic phase. These LCNPs fuse into the GUV membrane, increasing the excess membrane area and seeding the membrane with enhanced topological Gaussian curvature energy that lowers the energy barrier to the observed fission, fusion and tubulation processes. The interplay between these different morphological changes is summarised in Figure 6b.

The observations presented here are at a MO concentration of 1.4 mg/ml, which results in a MO/DOPC molar ratio of ~250. However, this is not the molar ratio of MO/DOPC in the mixed GUV membranes. The average swelling ratio of GUVs with an average diameter of 11±4 μm was found to be 19±11 % within 20 min of LCNP incubation

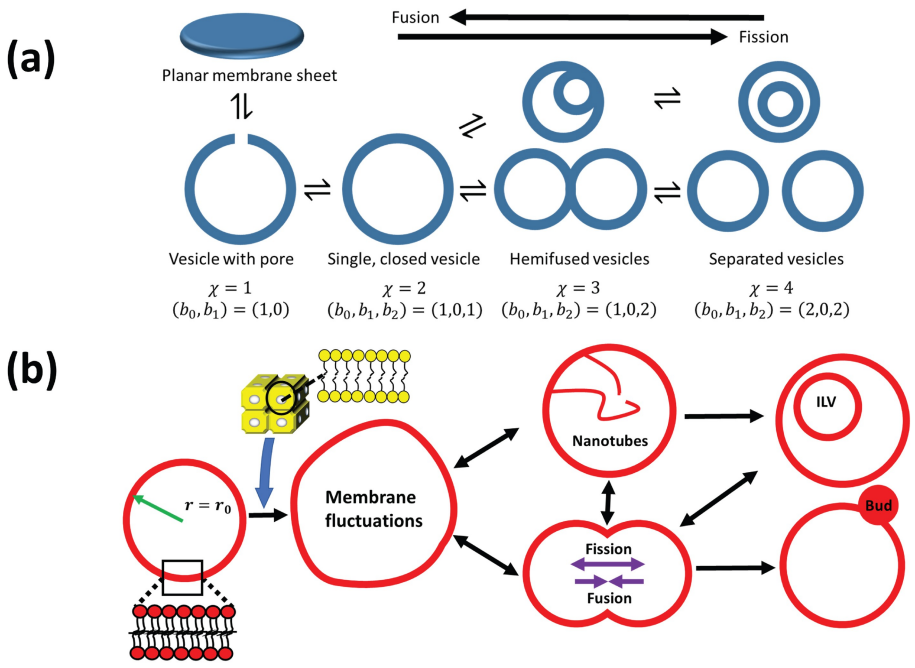

Figure 6. Topological transitions of vesicles and morphological changes observed in GUVs induced by LCNPs. (a) Common topology changes in vesicles with their Euler characteristic (χ) and Betti numbers (b_n). (b) Schematic representation of morphological changes of DOPC GUVs induced by MO-LCNPs (cubosomes).

(Table S1). Taking the molecular surface area of DOPC to be 0.67 nm^2,[22] and the polar molecular surface area of MO to be 0.33 nm^2,[23] we estimate the average molar ratio of MO in the GUV membrane to be 43 ± 17 mol %. Comparing our calculation to the phase diagram of MO/DOPC,[24] where equilibrium mixtures are found to be in the lamellar L_α phase up to ~75 mol % MO, we predict that these mixed systems are still in the lamellar phase of the equilibrium phase diagram within the studied time scale. At this ~43 mol % MO composition, the membranes dynamically undergo morphological transitions that re-equilibrate the GUVs by decreasing the excess membrane area until they return to their near-spherical final state. Note that fission and fusion events during the studied time scale will decrease or increase the swelling ratio, which might affect the calculated number of LCNPs incorporated per GUV.

At higher concentrations of MO-LCNPs, GUVs can become rapidly destabilised and destroyed. Here, the kinetics of MO incorporation into the GUV membrane will increase. We propose that under these conditions the increasing MO concentration in the membrane may pass the lamellar-cubic phase boundary (~75 mol % MO in the MO/DOPC membrane), where the faster kinetics of the lamellar to cubic phase transition occur before the slower dynamics of membrane topological and morphological transitions can occur.

While cubosome-vesicle interactions have been less commonly studied, several previous studies have investigated the interaction of detergents with lipid vesicles. Detergents have a cone-shape due to their relatively large hydrophilic head compared to their small hydrophobic volume (critical packing parameter <0.5), which induces a positive curvature stress in a membrane. This compares to MO, which has an inverted cone structure where the hydrophilic head is small compared to its bulkier hydrophobic tail region,[25] inducing negative curvature stress. The interaction of several detergents with different lipid membrane compositions have been reported, where the detailed mechanism of the interaction are dependent on the specific detergents and lipids used.[26] Detergents ultimately induce the breakdown of lipid vesicles into mixed lipid-detergent micelles.[26] This can occur through multiple different kinetic pathways, including gradual removal of lipids causing vesicle shrinkage, formation of large, open pores in the vesicle membrane and catastrophic vesicle rupture.[27] Critically, to the best of our knowledge, vesicle fission and fusion events have not been reported to be induced by the addition of detergents. This is indicative that these specific topological transitions require the generation of negative curvature stress (provided by MO) rather than the positive curvature stress induced by surfactants.

These fundamental new findings on the interaction of cubic phase LCNPs with lamellar GUV membranes will provide vital insights into a number of scientific questions and applications. Firstly, this approach might be able to provide new fundamental insight into the role of the Gaussian curvature modulus in vesicle fission and fusion.[28] By seeding lamellar GUVs with cubic phase forming lipids, the Gaussian curvature modulus of the GUV membrane might be controllably and systematically tuned. The major technical challenge with this approach is that the mechanical moduli of mixed membrane systems are not linearly additive based upon the moduli of each single lipid component in the mixture. Thus, a semi-quantitative approach may be the best strategy forward here.

Our approach holds promise for the bioengineering field of artificial cells. Dynamic topological changes such as fusion and fission are essential functional processes in living cells and hence are highly desirable features to engineer into minimal artificial cells.[29] To enhance this approach for the engineering biology toolbox, the leakage of GUV contents should be minimised to prevent loss of vital functional biomolecules from the GUV lumen, and further regulation of the interactions between LCNPs and GUVs might direct the morphological and topological transitions towards a specific mechanism (e.g., fusion, fission, ILV formation). Our findings here present important first steps in gaining control over membrane remodelling processes that will lead to simplified and enhanced mechanisms for regulating dynamic processes in artificial cell membranes.

Cubosomes are of interest for nanomedicine drug delivery systems.[4,12b, 30] Their high internal surface area gives a high potential drug loading capacity, but the higher curvature of cubic phase lipid assemblies is also thought to be relevant in inducing topological changes in the cell that facilitate cell entry and endosomal escape.[5h,9c, d, 30a, 31] Fundamental studies of LCNP-GUV interactions may assist with understanding different mechanisms of nanoparticle delivery in cells and also unwanted side effects of cell toxicity that needs to be minimised to facilitate translation to clinical applications.

Conclusion

Here we have presented new insights into the interactions of cubosomes with bilayer lipid membranes, important to our understanding of cubosomes as drug delivery systems and their application in other bioengineering technologies, such as synthetic biology. Our observations reveal a rich array of morphological and topological transitions driven by the kinetics of adsorption of MO-LCNPs into the lipid bilayer and equilibration processes within the GUV, once seeded with excess area and enhanced stored curvature stress in the membrane. The new insights and understanding we have presented in this study are not achievable in previous work on planar bilayer membranes, where the membrane dynamics are suppressed by a solid support, or in living cells, where deep mechanistic insight is frustrated by the complexity of living matter. Future exploration of the broad parameter space of the structure and composition of LCNPs and GUV membranes will promote optimisation of drug delivery and artificial cell technologies.

Correspondence and requests for materials should be addressed to A.I.I.T. and P.A.B.

Author contributions

Z.X., A.I.I.T., and P.A.B. conceived and designed the research. Z.X. performed the LCNPs experiments. A.I.I.T. and A.B. performed the MLVs experiments. Z.X and A.B. performed the FRAP experiment. Z.X. and M.P. performed and analysed the lattice light sheet experiments. Z.X. and A.I.I.T. collected and analysed the SAXS data. Z.X. analysed the remaining data. Z.X., M.R., A.I.I.T., and P.A.B. wrote the paper and interpreted the results. All authors revised and approved the final version of the manuscript.

Acknowledgements

We thank Dr Sally Boxall and Dr Ruth Hughes from the Bio-imaging and Flow Cytometry Facility at University of Leeds for their support on the confocal microscopes. We thank Dr Rebecca Thompson and Dr Daniel Maskell from the Astbury Biostructure Facility at University of Leeds for the assistance with Cryo-TEM. We thank Dr Rashmi Seneviratne and Dr Marcos Arribas Perez from School of Chemistry at University of Leeds for assistance on GUV preparation and fluorescence image analysis. We also thank Diamond Light Source for the award of beamtime (SM26258-1, SM19127) as well as Dr Sam Burholt, Dr Tim Snow, Dr Andy Smith and Professor Nick Terrill for their support and assistance. We further acknowledge the EPSRC as the funder of the Diamond Leeds SAXS facility (grant no. EP/R042683/1). The LSM880 + Airyscan confocal microscopes were funded by the Wellcome Trust (WT104918/Z/14/Z). The FEI Titan Krios microscope used was funded by the University of Leeds (UoL ABSL award) and Wellcome Trust (108466/Z/15/Z). We acknowledge the BBSRC Alert funding for the lattice light sheet microscope (BB/V01904X/1). The research was supported by start-up funding awarded to A.I.I.T. from the University of Leeds as a well as a PhD scholarship awarded to Z.X. P.A.B. and A.B. acknowledge funding from the Engineering and Physical Sciences Research Council (EPSRC: EP/M027929/1, EP/R03608X/1). The Bragg Centre for Materials Research at the University of Leeds is also acknowledged.

Conflict of Interest

The authors declare no competing interests.

Data Availability Statement

The data that support the findings of this study are available from the corresponding authors upon reasonable request.

Keywords: Artificial cells · cubosomes · lyotropic liquid crystal nanoparticles · membrane remodelling · vesicles

[1] a) G. van Meer, D. R. Voelker, G. W. Feigenson, *Nature Reviews Molecular Cell Biology* **2008**, *9*, 112; b) C. Klose, M. A. Surma, K. Simons, *Current Opinion in Cell Biology* **2013**, *25*, 406; c) Z. A. Almsherqi, S. D. Kohlwein, Y. Deng, *Journal of Cell Biology* **2006**, *173*, 839.

[2] a) J. Zhai, C. Fong, N. Tran, C. J. Drummond, *ACS Nano* **2019**, *13*, 6178; b) R. Tenchov, R. Bird, A. E. Curtze, Q. Zhou, *ACS Nano* **2021**, *15*, 16982; c) M. L. Guevara, F. Persano, S. Persano, *Frontiers in Chemistry* **2020**, *8*, 963.

[3] a) L. van't Hag, S. L. Gras, C. E. Conn, C. J. Drummond, *Chemical Society Reviews* **2017**, *46*, 2705; b) J. N. Israelachvili, D. J. Mitchell, B. W. Ninham, *Journal of the Chemical Society, Faraday Transactions 2: Molecular and Chemical Physics* **1976**, *72*, 1525.

[4] H. M. G. Barriga, M. N. Holme, M. M. Stevens, *Angewandte Chemie International Edition* **2019**, *58*, 2958.

[5] a) C. Leal, N. F. Bouxsein, K. K. Ewert, C. R. Safinya, *J Am Chem Soc* **2010**, *132*, 16841; b) D. P. Siegel, R. M. Epand, *Biophys J* **1997**, *73*, 3089; c) C. Leal, K. K. Ewert, R. S. Shirazi, N. F. Bouxsein, C. R. Safinya, *Langmuir* **2011**, *27*, 7691; d) L. Yang, H. W. Huang, *Science* **2002**, *297*, 1877; e) D. P. Siegel, *Chemistry and Physics of Lipids* **1986**, *42*, 279; f) I. D. M. Azmi, P. P. Wibroe, L.-P. Wu, A. I. Kazem, H. Amenitsch, S. M. Moghimi, A. Yaghmur, *Journal of Controlled Release* **2016**, *239*, 1; g) L. Chernomordik, M. M. Kozlov, J. Zimmerberg, *The Journal of Membrane Biology* **1995**, *146*, 1; h) H. Yu, A. Angelova, B. Angelov, B. Dyett, L. Matthews, Y. Zhang, M. El Mohamad, X. Cai, S. Valimehr, C. J. Drummond, J. Zhai, *Angewandte Chemie International Edition* **2023**, *62*, e202304977.

[6] a) R. L. Knorr, N. Mizushima, R. Dimova, *Traffic* **2017**, *18*, 758; b) J. G. Carlton, H. Jones, U. S. Eggert, *Nature Reviews Molecular Cell Biology* **2020**, *21*, 151; c) J. M. Kalappurakkal, P. Sil, S. Mayor, *Protein Sci* **2020**, *29*, 1355; d) T. H. Ogunmowo, H. Jing, S. Raychaudhuri, G. F. Kusick, Y. Imoto, S. Li, K. Itoh, Y. Ma, H. Jafri, M. B. Dalva, E. R. Chapman, T. Ha, S. Watanabe, J. Liu, *Nat Commun* **2023**, *14*, 2888.

[7] a) H. T. McMahon, J. L. Gallop, *Nature* **2005**, *438*, 590; b) A.-L. Le Roux, C. Tozzi, N. Walani, X. Quiroga, D. Zalvidea, X. Trepat, M. Staykova, M. Arroyo, P. Roca-Cusachs, *Nature Communications* **2021**, *12*, 6550; c) J. H. Hurley, S. D. Emr, *Annual Review of Biophysics and Biomolecular Structure* **2006**, *35*, 277; d) S. Mayor, R. E. Pagano, *Nature Reviews Molecular Cell Biology* **2007**, *8*, 603; e) T. Wang, L. Li, W. Hong, *Traffic* **2017**, *18*, 767.

[8] a) T. Harayama, H. Riezman, *Nature Reviews Molecular Cell Biology* **2018**, *19*, 281; b) D. Lingwood, K. Simons, *Science* **2010**, *327*, 46; c) E. Sezgin, I. Levental, S. Mayor, C. Eggeling, *Nature Reviews Molecular Cell Biology* **2017**, *18*, 361; d) J. H. Lorent, K. R. Levental, L. Ganesan, G. Rivera-Longsworth, E. Sezgin, M. Doktorova, E. Lyman, I. Levental, *Nat Chem Biol* **2020**, *16*, 644.

[9] a) D. P. Chang, J. Barauskas, A. P. Dabkowska, M. Wadsäter, F. Tiberg, T. Nylander, *Advances in Colloid and Interface Science* **2015**, *222*, 135; b) B. P. Dyett, H. Yu, S. Sarkar, J. B. Strachan, C. J. Drummond, C. E. Conn, *ACS Applied Materials & Interfaces* **2021**, *13*, 53530; c) B. P. Dyett, H. Yu, J. Strachan, C. J. Drummond, C. E. Conn, *Nat Commun* **2019**, *10*, 4492; d) L. Zheng, S. R. Bandara, Z. Tan, C. Leal, *Proceedings of the National Academy of Sciences* **2023**, *120*, e2301067120; e) I. S. Zuhorn, U. Bakowsky, E. Polushkin, W. H. Visser, M. C. A. Stuart, J. B. F. N. Engberts, D. Hoekstra, *Molecular Therapy* **2005**, *11*, 801; f) R. Pattipeiluhu, Y. Zeng, M. M. R. M. Hendrix, I. K. Voets, A. Kros, T. H. Sharp, *Nature Communications* **2024**, *15*, 1303; g) S. Pushpa Ragini, B. P. Dyett, S. Sarkar, J. Zhai, J. F. White, R. Banerjee, C. J. Drummond,

C. E. Conn, *Journal of Colloid and Interface Science* **2024**, *663*, 82.
[10] a) P. Vandoolaeghe, A. R. Rennie, R. A. Campbell, T. Nylander, *Langmuir* **2009**, *25*, 4009; b) P. Vandoolaeghe, A. R. Rennie, R. A. Campbell, R. K. Thomas, F. Höök, G. Fragneto, F. Tiberg, T. Nylander, *Soft Matter* **2008**, *4*, 2267.
[11] P. Vandoolaeghe, J. Barauskas, M. Johnsson, F. Tiberg, T. Nylander, *Langmuir* **2009**, *25*, 3999.
[12] a) S. L. Yap, H. Yu, S. Li, C. J. Drummond, C. E. Conn, N. Tran, *Journal of Colloid and Interface Science* **2024**, *656*, 409; b) H. Azhari, M. Younus, S. M. Hook, B. J. Boyd, S. B. Rizwan, *International Journal of Pharmaceutics* **2021**, *600*, 120411; c) J. Iscaro, H. Yu, N. Martinez, S. Subramaniam, P. Joyce, H. Wang, B. P. Dyett, J. White, C. A. Prestidge, C. J. Drummond, S. Bozinovski, J. Zhai, *Advanced Functional Materials* **2024**, n/a, 2405286; d) J. Caukwell, S. Assenza, K. A. Hassan, B. A. Neilan, A. J. Clulow, L. Salvati Manni, W.-K. Fong, *Journal of Colloid and Interface Science* **2025**, *677*, 293.
[13] a) A. M. Falchi, A. Rosa, A. Atzeri, A. Incani, S. Lampis, V. Meli, C. Caltagirone, S. Murgia, *Toxicology Research* **2015**, *4*, 1025; b) A. Rosa, S. Murgia, D. Putzu, V. Meli, A. M. Falchi, *Chemistry and Physics of Lipids* **2015**, *191*, 96; c) J. B. Strachan, B. P. Dyett, Z. Nasa, C. Valery, C. E. Conn, *J Colloid Interface Sci* **2020**, *576*, 241.
[14] P. Vandoolaeghe, R. A. Campbell, A. R. Rennie, T. Nylander, *The Journal of Physical Chemistry C* **2009**, *113*, 4483.
[15] a) C. L. Bergstrom, P. A. Beales, Y. Lv, T. K. Vanderlick, J. T. Groves, *Proceedings of the National Academy of Sciences* **2013**, *110*, 6269; b) J. Heuvingh, S. Bonneau, *Biophysical Journal* **2009**, *97*, 2904.
[16] M. K. Dymond, R. J. Gillams, D. J. Parker, J. Burrell, A. Labrador, T. Nylander, G. S. Attard, *Langmuir* **2016**, *32*, 10083.
[17] B. Kollmitzer, P. Heftberger, M. Rappolt, G. Pabst, *Soft Matter* **2013**, *9*, 10877.
[18] S. Chaïeb, S. Rica, *Physical Review E* **1998**, *58*, 7733.
[19] R. Lipowsky, *Advanced Biology* **2022**, *6*, 2101020.
[20] P. Pranav, R. van de Weygaert, G. Vegter, B. J. T. Jones, R. J. Adler, J. Feldbrugge, C. Park, T. Buchert, M. Kerber, *Monthly Notices of the Royal Astronomical Society* **2019**, *485*, 4167.
[21] V. Tchakalova, T. Zemb, F. Testard, *The Journal of Chemical Physics* **2022**, *157*.
[22] N. Kucerka, J. F. Nagle, J. N. Sachs, S. E. Feller, J. Pencer, A. Jackson, J. Katsaras, *Biophys J* **2008**, *95*, 2356.
[23] R. H. Templer, *Langmuir* **1995**, *11*, 334.
[24] V. Cherezov, J. Clogston, Y. Misquitta, W. Abdel-Gawad, M. Caffrey, *Biophys J* **2002**, *83*, 3393.
[25] C. V. Kulkarni, W. Wachter, G. Iglesias-Salto, S. Engelskirchen, S. Ahualli, *Physical Chemistry Chemical Physics* **2011**, *13*, 3004.
[26] F. Nomura, M. Nagata, T. Inaba, H. Hiramatsu, H. Hotani, K. Takiguchi, *Proceedings of the National Academy of Sciences* **2001**, *98*, 2340.
[27] a) M. C. A. Stuart, E. J. Boekema, *Biochimica et Biophysica Acta (BBA) - Biomembranes* **2007**, *1768*, 2681; b) T. P. Sudbrack, N. L. Archilha, R. Itri, K. A. Riske, *The Journal of Physical Chemistry B* **2011**, *115*, 269; c) K. Edwards, M. Almgren, *Journal of Colloid and Interface Science* **1991**, *147*, 1.
[28] P. Bassereau, R. Jin, T. Baumgart, M. Deserno, R. Dimova, V. A. Frolov, P. V. Bashkirov, H. Grubmüller, R. Jahn, H. J. Risselada, L. Johannes, M. M. Kozlov, R. Lipowsky, T. J. Pucadyil, W. F. Zeno, J. C. Stachowiak, D. Stamou, A. Breuer, L. Lauritsen, C. Simon, C. Sykes, G. A. Voth, T. R. Weikl, *Journal of Physics D: Applied Physics* **2018**, *51*, 343001.
[29] a) M. Arribas Perez, P. A. Beales, *Langmuir* **2021**, *37*, 13917; b) N. Y. Kostina, A. M. Wagner, T. Haraszti, K. Rahimi, Q. Xiao, M. L. Klein, V. Percec, C. Rodriguez-Emmenegger, *Soft Matter* **2021**, *17*, 254; c) Y. Dreher, K. Jahnke, E. Bobkova, J. P. Spatz, K. Göpfrich, *Angewandte Chemie International Edition* **2021**, *60*, 10661; d) R. B. Lira, T. Robinson, R. Dimova, K. A. Riske, *Biophysical Journal* **2019**, *116*, 79; e) M. Reverte-López, N. Kanwa, Y. Qutbuddin, M. Jasnin, P. Schwille, *bioRxiv* **2024**, *2024*.06.17.599291; f) S. Kohyama, A. Merino-Salomón, P. Schwille, *Nature Communications* **2022**, *13*, 6098.
[30] a) J. A. Prange, S. Aleandri, M. Komisarski, A. Luciani, A. Käch, C.-D. Schuh, A. M. Hall, R. Mezzenga, O. Devuyst, E. M. Landau, *ACS Applied Bio Materials* **2019**, *2*, 2490; b) A. Pramanik, Z. Xu, S. H. Shamsuddin, Y. S. Khaled, N. Ingram, T. Maisey, D. Tomlinson, P. L. Coletta, D. Jayne, T. A. Hughes, A. I. I. Tyler, P. A. Millner, *ACS Appl Mater Interfaces* **2022**, *14*, 11078; c) A. Pramanik, Z. Xu, N. Ingram, P. L. Coletta, P. A. Millner, A. I. I. Tyler, T. A. Hughes, *Mol Pharm* **2022**, *19*, 4601.
[31] a) H. Kim, C. Leal, *ACS Nano* **2015**, *9*, 10214; b) S. Deshpande, N. Singh, *Langmuir* **2017**, *33*, 3509; c) H. Kim, J. Sung, Y. Chang, A. Alfeche, C. Leal, *ACS Nano* **2018**, *12*, 9196; d) J. Philipp, A. Dabkowska, A. Reiser, K. Frank, R. Krzysztoń, C. Brummer, B. Nickel, C. E. Blanchet, A. Sudarsan, M. Ibrahim, S. Johansson, P. Skantze, U. Skantze, S. Östman, M. Johansson, N. Henderson, K. Elvevold, B. Smedsrød, N. Schwierz, L. Lindfors, J. O. Rädler, *Proceedings of the National Academy of Sciences* **2023**, *120*, e2310491120; e) H. Yu, J. Iscaro, B. Dyett, Y. Zhang, S. Seibt, N. Martinez, J. White, C. J. Drummond, S. Bozinovski, J. Zhai, *Journal of the American Chemical Society* **2023**, *145*, 24765.

Manuscript received: August 6, 2024
Accepted manuscript online: September 30, 2024
Version of record online: December 17, 2024